Exciting and confining light in Cr doped gallium oxide

M. Alonso-Orts, E. Nogales, José M. San Juan, María L. Nó, Bianchi Méndez

M. Alonso-Orts, E. Nogales, José M. San Juan, María L. Nó, Bianchi Méndez, "Exciting and confining light in Cr doped gallium oxide," Proc. SPIE 10919, Oxide-based Materials and Devices X, 109191S (1 March 2019); doi: 10.1117/12.2509672

SPIE.

Event: SPIE OPTO, 2019, San Francisco, California, United States

Exciting and confining light in Cr doped gallium oxide

M. Alonso-Orts[a], E. Nogales[a], José M. San Juan[b], María L. Nó [c], Bianchi Méndez*[a]

[a] Departamento de Física de Materiales, Facultad de Ciencias Físicas, Universidad Complutense de Madrid, 28040-Madrid, Spain
[b] Departamento de Física de la Materia Condensada, Facultad de Ciencias y Tecnología, Universidad del País Vasco, Apdo. 644, 48080, Bilbao, Spain
[c] Departamento Física Aplicada II, Facultad de Ciencia y Tecnología, Universidad del País Vasco, Apdo. 644, 48080 Bilbao, Spain

ABSTRACT

On one hand, interest on the tunability of the optical microcavities has increased in the last few years due to the need for selective nano- and microscale light sources to be used as photonic building blocks in several applications. On the other, transparent conductive oxide (TCO) β-Ga_2O_3 is attracting attention in the optoelectronics area due to its ultra wide band gap and high breakdown field. However, at the micro- and nanoscale there are still some challenges to face up, namely the control and tuning of the optical and electrical properties of this oxide.

In this work, Cr doped Ga_2O_3 elongated microwires are grown using the vapor-solid (VS) mechanism. Focused Ion Beam (FIB) etching forms Distributed Bragg Reflector (DBR)-based resonant microcavities. Room temperature micro-photoluminescence (μ-PL) spectra show strong modulations in the red-NIR range on five cavities with different lengths. Selectivity of the peak wavelengths is obtained, proving the tunability of this kind of optical systems. The confined modes are analyzed experimentally, analytically and via finite difference time domain (FDTD) simulations. Experimental reflectivities up to 78% are observed.

Keywords: Resonant modes, gallium oxide, DBR, optical microcavities, tunability

1. INTRODUCTION

The use of micro- and nanowires as elements in photonic devices has been a hot issue of significant research recently. In particular, optical microcavities are key elements in such devices, and have been developed for applications in optical filters, lasers[1] or biosensors[2], among others. Different configurations have been used to guide and confine light inside semiconductor microcavities. In particular, DBR-based microcavities can be created by FIB etching[3] and the high refractive index contrast in these periodic patterns results in shorter device lengths than in other configurations. In addition, DBRs allow tunability on the resonant wavelengths, as the stop band resulting from the periodic pattern can be selected on the whole optical range depending on the DBR parameters[4].

Among the possible materials to be used for optical microcavities, β-Ga_2O_3 is of high interest. This oxide combines a very high breakdown field with a wide tunable PL range, spanning from the UV to the IR depending on the dopant used[5,6]. We have studied waveguiding and confinement on Cr doped Ga_2O_3 microwires in the past decade[7-10]. In addition to the phonon-assisted red-NIR broad band and the R-lines[7], low quality modulations due Fabry-Perot reflections in the wire ends were demonstrated[9]. With the objective of improving their reflectivity and tuning their resonances in the broad red-NIR range, DBR-based Ga_2O_3:Cr optical microcavities have been very recently developed and their resonant modes have been thoroughly studied[10]. These microcavities dramatically enhance their optical performance in comparison to the unpatterned microwires. However, size reduction[11] and further improvement on the photon lifetimes, i.e the finesse, of these cavities is needed in order to increase their potential applications. In this work, in the optical performance and tunability range of Cr doped Ga_2O_3, DBR-based microcavities is further studied and improved via polarized μ-PL measurements, theoretical models and FDTD simulations.

*bianchi@fis.ucm.es; www.finegroup.es

Oxide-based Materials and Devices X, edited by David J. Rogers, David C. Look, Ferechteh H. Teherani, Proc. of SPIE Vol. 10919, 109191S · © 2019 SPIE
CCC code: 0277-786X/19/$18 · doi: 10.1117/12.2509672

2. EXPERIMENTAL

Cr doped Ga_2O_3 microwires were fabricated in a single step thermal treatment[9]. EDX measurements revealed Cr cation atomic concentration in the range of 0.5 at. %. Some microwires were deposited on a holey carbon TEM grid so that they were suspended in air, except for the carbon "mesh". DBR patterns were milled by FIB in a FEI Helios 650 at 30 kV and 24 pA for the ion column, in order to optimize the sharpness of the features, as analyzed in previous milling work[12]. The design of the DBR dimensions was made by FDTD simulations performed with OptiFDTD software. Ga_2O_3 has to be considered a dispersive medium in the wavelength range of interest because $(\omega/n)(dn/d\omega)$ is around 0.1 for the current frequencies. Therefore, Sellmeier dispersion relation $\varepsilon = A + \frac{B\lambda^2}{\lambda^2 - C^2}$ has been used, with parameters A = 2.31, B = 1.14 and C = 0.24 obtained from fitting Sellmeier expression to experimental data from Al-Kuhaili et al[13]. Morphology and actual dimensions of the FIB patterns were analyzed either with a FEI Inspect or a JEOL JSM 7600F SEM. Room temperature μ-PL spectra were acquired in a Horiba Jobin-Yvon LabRam 800 confocal microscope system with a Kimmon HeCd laser, λ_{exc} = 325 nm, as excitation source. This system allows exciting with the laser in a position different from that of the detection point.

3. RESULTS AND DISCUSSION

Figure 1(a) shows the general design of the optical microcavities: using a FIB, N rectangular holes, of length α and periodicity Λ, are drilled in both sides, leaving in between cavities of length L. Figure 1(b) shows microwire 1, in which two cavities of similar lengths, L_{1A} = 15.2 μm and L_{1B} = 15.0 μm, but with a DBR having a different number of periods, N = 20 in cavity 1A and N = 10 in cavity 1B, were fabricated. This microwire was analyzed previously on ref. 10. Figure 1(c) shows microwire 2, in which three cavities of lengths L_{2A} = 4.9 μm, L_{2B} = 13.0 μm and L_{2C} = 5.9 μm and same number of periods, N = 10, are fabricated. Figure 1(d) shows a high magnification image of microwire 2, tilted 33º. From this image, we obtain the value of the microwire thickness: b = 620 nm. Besides, at least one edge is seen on the lateral sides, indicating that the cross section is not rectangular. This also happens on microwire 1[10], where the cross section is an irregular hexagon. For simplicity, we also make this assumption on microwire 2. A sketch of the assumed cross section of microwire 2 is shown in figure 1(e). As shown in figures 1(a) and 1(e), two parameters describe the top view of the nanowire: a is the total width as seen from the SEM while a_t is the top face of the hexagon. Similar microwire cross sections, ranging from hexagonal to more faceted, on Ga_2O_3 micro- and nanowires grown by vapor-solid have been reported[14].

The dimensions of both microwires and their FIB patterns are shown in table I. As it can be seen, microwire 2 has a smaller cross section than microwire 1, the microcavities designed for microwire 2 have shorter lengths than for microwire 1 and all three cavities on microwire 2 are made by 10-period DBRs. All this data indicates an improvement in the size reduction of these optical cavities.

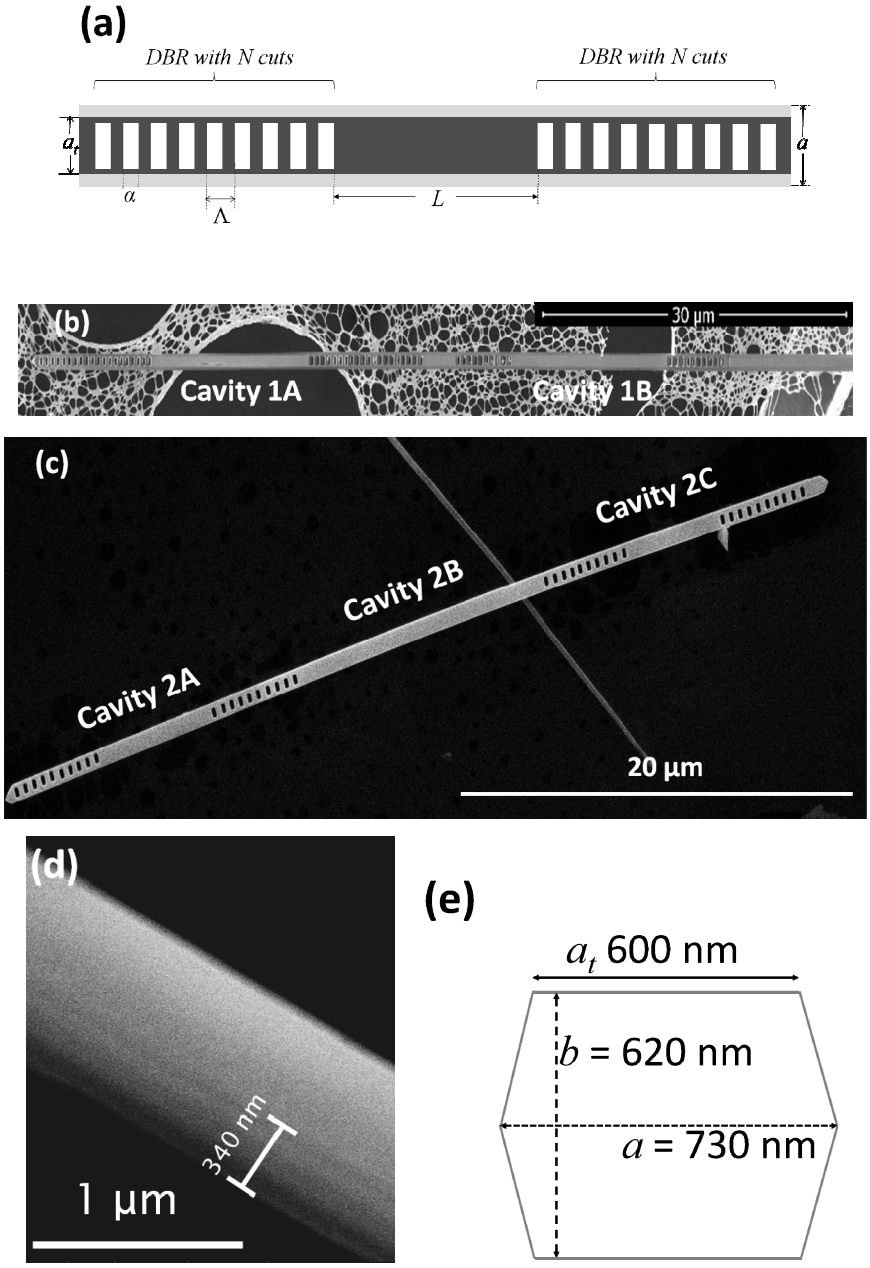

Figure 1. (a) Schematic of the different cavity parameters. Top view SEM image of the optical cavities patterned on (b) microwire 1 (c) microwire 2. (d) Top view detail of microwire 2 at 33º tilt. (e) Sketch of the cross section of microwire 2. A similar sketch applies to microwire 1, but with different a, b and a_t values, as shown on table I.

Microwire	a (nm)	a_t (nm)	b (nm)	L (µm)	α (nm)	Λ (nm)
1	1150	760	510	15.2 and 15.0	210	520
2	730	600	620	5.9, 13.0 and 4.9	190	470

Table I: Comparison of the cavities' parameters. The cavity lengths are indicated following the order of the cavities, i.e L_{2A}=5.9 µm, L_{2B}=13.0 µm and L_{2C}=13.0 µm. For the meaning of each parameter, check figures 1(a) and 1(e).

Micro-photoluminescence (μ-PL) analysis from the unpatterned microwires as well as from the five cavities has been performed in the confocal microscope. Before patterning, luminescence spectra due to excitation with the UV laser (λ_{exc} = 325 nm) are detected locally from one end of the structure of interest. After patterning, detection is performed on a different point to excitation, as explained elsewhere[9,10]. Figure 2(a) shows the room-temperature μ-PL image from cavity 2B in these conditions. White dotted lines indicate the wire and DBR positions, for the sake of clarity. In addition, axes are defined: *z* is parallel to the cavity longitudinal axis (propagation direction), and the transversal axis shown on the PL image is the x axis. The y axis, perpendicular to both, is the optical axis.

Spectra from the unpatterned Ga_2O_3:Cr microwires are shown in figure 2(b). Both present the characteristic red emission due to the incorporation of trivalent chromium ions on this host[7]. No modulations are seen apart from very weak Fabry-Perot resonances due to reflectivity between the wire ends on microwire 1. On the other hand, strong modulations are observed on all five designed cavities, as shown on the μ-PL spectra on figures 2(c)-(g). For all the spectra, a polarizer was placed with its axis parallel to the x axis, i.e. perpendicular to the light propagation direction within the wire.

A strong polarization dependence of the resonant modes is observed in these cavities, which can be studied analytically by Marcatili and Goell models, as explained elsewhere[10]. In these models, the cavity modes can be divided into two sets depending on their polarization: E^x_{pq} and E^y_{pq}. The E^x_{pq} modes are defined by having $H_x = 0$, while E_x and H_y dominate. In order to filter them from the E^y_{pq} modes, the polarizer is placed between the microwire and the CCD detector as explained above: its axis parallel to x. In this paper we focus on the most intense propagation mode from this set: the fundamental E^x_{11} mode. For this mode, the dispersion equations for a rectangular waveguide surrounded by air are as follows:

$$\left.\begin{aligned} k_x \frac{a}{2} &= \arctan\left(\frac{n^2\sqrt{k_0^2(n^2-1)-k_x^2}}{k_x}\right) \\ k_y \frac{b}{2} &= \arctan\left(\frac{\sqrt{k_0^2(n^2-1)-k_y^2}}{k_y}\right) \\ k_z^2 &= k_0^2 n^2 - k_x^2 - k_y^2 \end{aligned}\right\} \quad (1)$$

Where k_x, k_y and k_z are the wavevector components in the waveguide, *a* and *b* are the waveguide transversal dimensions, *n* is the refractive index and k_0 is the vacuum wavenumber. The obtained k_z values for each peak must also fulfill the longitudinal resonance condition along the cavity axis:

$$k_z = l\frac{\pi}{L_{eff}} \quad (2)$$

Where *l* are consecutive integers for consecutive peaks. Excellent fits are obtained for the most intense resonance peaks in this polarization when assigned to the E^x_{11} mode in all cavities, both for microwire 1[10] and microwire 2. The identified modulations assigned to E^x_{11} modes for the five cavities are shown in figures 2(c) to 2(g) with blue dashed lines. Note that the low cavity lengths of microwire 2 give rise to only 3 and 5 resonant peaks on the 680-750 nm range for cavities 2C and 2A respectively. This is an improvement from previous works on these cavities towards the single-mode regime.

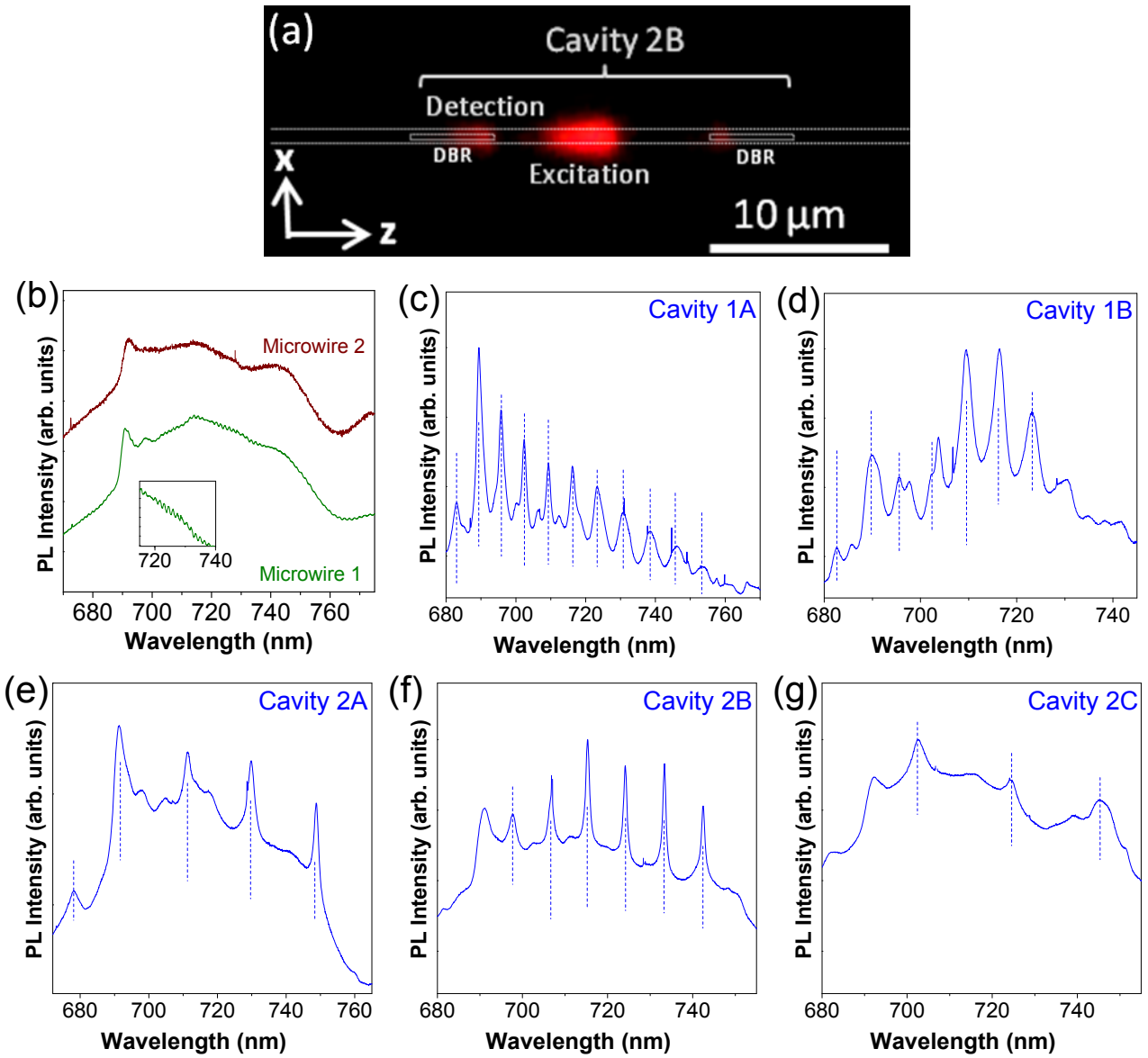

Figure 2. (a) µ-PL image of cavity 2B indicating the excitation and detection points. White dotted lines represent the waveguide and the patterned DBRs, shown in fig. 1(c). (b) Normalized µ-PL spectra from unpatterned microwires 1 and 2. µ-PL spectra from (c) cavity 1A, (d) cavity 1B, (e) cavity 2A, (f) cavity 2B, and (f) cavity 2C. All cavity spectra are acquired with the polarizer's axis parallel to the x axis, i.e perpendicular to the light propagation direction within the wire. Dashed blue lines show the identified E_x^{11} resonances.

In order to compare the performance of the DBR cavities, reflectivity (R) values are obtained. Firstly, finesse (F) values corresponding to the wavelength of each peak can be obtained from the ratio of the full width at half maximum (FWHM) of one peak $\Delta\nu_{FWHM}$ and the free spectral range between this peak and the next one $\delta\nu_{FSR}$. Secondly, assuming R is the same for the two DBRs that form each cavity, from the experimental F values, R is obtained by rearranging $F = \frac{\pi\sqrt{R}}{1-R}$ [15].

The reflectivity of a DBR depends strongly on the incident wavelength; hence F and R values vary throughout the PL emission range. A comparison between the top two reflectivity values for the three cavities in microwire 2 and the best

performing cavity in microwire 1 (cavity 1A) on the 650-800 nm range is shown on table II. All three cavities in microwire 2 have better average reflectivity values in comparison to those in microwire 1. The highest reflectivity, 78%, is obtained for cavity 2A. This value is more than 10% higher than the highest reflectivity obtained for cavities on microwire 1, despite the reduction from $N = 20$ to $N = 10$ periods in the DBR. In addition, the highest reflectivities lie on the most intense PL wavelength range, namely the 725-750 nm range.

Cavity 1A		Cavity 2A		Cavity 2B		Cavity 2C	
λ (nm)	R	λ (nm)	R	λ (nm)	R	λ (nm)	R
798	0.66	749	0.78	733	0.73	725	0.76
709	0.55	730	0.69	742	0.71	703	0.64

Table II: Comparison of the highest experimental reflectivities, calculated from the finesse of individual peaks, between cavities 1A, 2A, 2B and 2C.

In order to further understand and optimize the DBR cavities, FDTD simulations have been carried out using the commercial OptiFDTD software. The experimentally determined dimensions and actual cross-section of the two microwires, as well as those of the fabricated DBRs (see table I) have been implemented for the simulations. Figure 3(a) shows the design for microwire 2. A 10-period DBR with α=210 nm, Λ=470 nm is placed after an incident pulse. This pulse is a Gaussian wave centered on 740 nm which will be partly reflected by the DBR. Detection planes are placed both before the pulse and after the DBR, detecting the reflected and transmitted wave respectively. The reflection and transmission spectra of the DBR designed for microwire 2 is shown in figure 3(b). Superimposed are the main experimental reflectivities of each cavity. The simulations agree with experimental data, showing a stop band on the 700-750 nm range. Note that reflectivity is also high on the 680-700 nm range, see figure 2, but the Cr^{3+} R-lines at 691 and 698 nm prevent any precise calculations of finesse values in that range. Experimental and simulated reflectivity values are closer in magnitude in this microwire 2 than in microwire 1[10], proving an improved FIB implementation of the designed cavities.

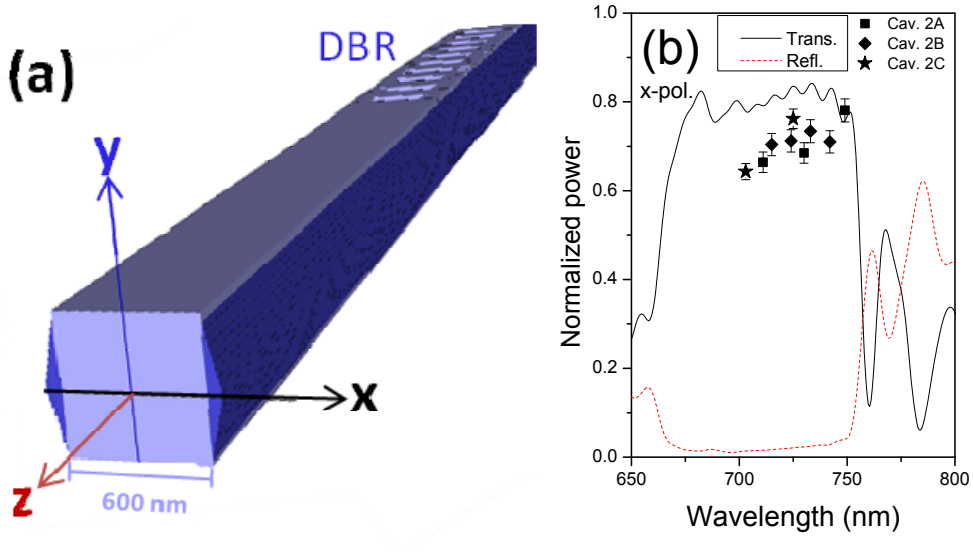

Figure 3. (a) Side view of the simulated DBR for microwire 2. An incident pulse is placed just before the sets of holes and detection planes are placed before and after the DBR in order to obtain the reflected and transmitted spectra. The axes are defined like in fig. 2(a). (b) FDTD-simulated reflected power spectrum for x polarization on one DBR of microwire 2. Black squares (cavity 2A), black rhombi (cavity 2B) and black stars (cavity 2C) show experimental R values obtained from finesse calculations (table II). Transmitted spectrum is shown in dashed red lines.

4. CONCLUSIONS

Cr-doped gallium oxide microwires have been patterned by FIB etching in order to obtain tunable, high-reflectivity DBR-based microcavities. Five microcavities of different lengths have been analyzed, and they display intense resonances in the Ga_2O_3:Cr red-NIR range. Their performance is compared experimentally, analytically and by simulations. The cavities from microwire 2 have smaller dimensions and show better reflectivity and tunability than microwire 1. Reflectivity values up to 78% were obtained on the 700-750 nm range from the experimental analysis , in good agreement with the FDTD simulations. On the other hand, the positions of the resonance peaks agree with the analytical models needed for the geometry of the microwires.

ACKNOWLEDGEMENTS

The authors are grateful for the financial support from the MINECO (Projects No. MAT-2015-65274-R-FEDER and PCIN-2017-106). M. A.-O. acknowledges financial support from MICINN (FPU Contract No. FPU15/01982).

REFERENCES

[1] Hill, M. T. and Gather, M. C., "Advances in small lasers," Nat. Photonics 8, 908 (2014).
[2] Guo, Q., Zhu, H., Liu, F., Zhu, A. Y., Reed, J. C., Yi, F. and Cubukcu, E., "Silicon-on-glass graphene-functionalized leaky cavity mode nanophotonic biosensor," ACS Photonics 1, 221 (2014).
[3] Alias, M. S., Dursun, I., Shi, D., Saidaminov, M. I., Diallo, E. M., Priante, D., Ng, T. K., Bakr, O. M. and Ooi, B. S., "Focused-ion beam patterning of organolead trihalide perovskite for subwavelength grating nanophotonic applications." Jour. Vac. Sci Technol. B, 33(5), 051207 (2015).
[4] Fu, A., Gao, H., Petrov, P. and Yang, P., "Widely Tunable Distributed Bragg Reflectors Integrated into Nanowire Waveguides," Nano Lett. 15, 6909 (2015).
[5] Nogales, E., Garcia, J. A., Mendez, B. and Piqueras, J., "Doped gallium oxide nanowires with waveguiding behavior," Appl. Phys. Lett. 91, 133108 (2007).
[6] Nogales, E., López, I., Méndez, B., Piqueras, J., Lorenz, K., Alves, E. and García, J. A., "Doped gallium oxide nanowires for photonics," Proc. SPIE 8263, 82630B (2012).
[7] Nogales, E., Garcia, J.A., Mendez, B. and Piqueras, J., "Red luminescence of Cr in β-Ga_2O_3 nanowires," J. Appl. Phys. 101, 033517 (2007).
[8] Méndez, B., Cebriano, T., López, I., Nogales, E. and Piqueras, J., "Waveguiding and confinement of light in semiconductor oxide microstructures," Proc. SPIE 8626, 86260T (2013).
[9] Lopez, I., Nogales, E., Mendez, B. and Piqueras, J., "Resonant cavity modes in gallium oxide microwires," Appl. Phys. Lett. 100, 261910 (2012).
[10] Alonso-Orts, M., Nogales, E., San Juan, J. M., Nó, M. L., Piqueras, J. and Méndez, B., "Modal Analysis of β−Ga2O3:Cr Widely Tunable Luminescent Optical Microcavities," Phys. Rev. Appl. 9(6), 064004 (2018).
[11] Eaton, S. W., Fu, A., Wong, A. B., Ning, C. Z. and Yang, P., "Semiconductor nanowire lasers," Nat. Rev. Mater. 1(6), 16028 (2016).
[12] Gomez-Cortes, J. F., No, M. L., Lopez-Ferreño, I., Hernandez-Saz, J., Molina, S. I., Chuvilin, A. and San Juan, J. M., "Size effect and scaling power-law for superelasticity in shape-memory alloys at the nanoscale," Nat. Nanotechnol. 12, 790 (2017).
[13] Al-Kuhaili, M. F, Durrani, S. M. A. and Khawaja, E. E., "Optical properties of gallium oxide films deposited by electron-beam evaporation," Appl. Phys. Lett. 83**,** 4533 (2003).
[14] Hosein, I. D., Hegde, M., Jones, P. D., Chirmanov, V. and Radovanovic, P. V., "Evolution of the faceting, morphology and aspect ratio of gallium oxide nanowires grown by vapor–solid deposition," J. Cryst. Growth 396, 24-32 (2014).
[15] Suter, M. and Dietiker, P., "Calculation of the finesse of an ideal Fabry–Perot resonator," Appl. Opt. 53, 7004 (2014).